ENT Updates
https://ojs.ukscip.com/index.php/ENTU

Article

RAD54-Like Protein 2 Is a Potential Diagnostic and Prognostic Biomarker in Head and Neck Squamous Cell Carcinoma

Xingnong Xu [1,2] **and Lei Ma** [1,*]

[1] School of Pharmacy, East China University of Science and Technology, Shanghai 200237, China

[2] Department of Pharmacy, Yancheng Third People's Hospital, Affiliated Hospital 6 of Nantong University, Yancheng 224000, China

[*] Correspondence: malei@ecust.edu.cn

Received: 21 September 2025; **Revised:** 12 November 2025; **Accepted:** 20 November 2025; **Published:** 2 December 2025

Abstract: Head and Neck Squamous Cell Carcinoma (HNSCC) poses a major global health challenge, highlighting the demand for reliable biomarkers to enable earlier detection and improve patient survival. This study sought to evaluate the diagnostic and prognostic significance of RAD54-like Protein 2 (RAD54L2) in HNSCC. RAD54L2 expression was assessed across multiple cancer types, including HNSCC, using data sourced from The Cancer Genome Atlas (TCGA) and Gene Expression Omnibus (GEO). Through R-based analysis of RNA-seq data from TCGA-HNSCC, differentially expressed genes (DEGs) were identified between tumors with high and low RAD54L2 expression. RAD54L2 may be a useful diagnostic and prognostic biomarker in HNSCC. Using various statistical methods, we explored the relationship between RAD54L2 levels and immune cell infiltration, DNA methylation patterns and genetic alterations in RAD54L2, RAD54L2 expression with clinicopathological features of HNSCC patients, and the diagnostic and prognostic utility of RAD54L2. Its expression was markedly upregulated in tumor tissues versus controls. RAD54L2 expression exhibited significant correlations with immune infiltration, cell cycle genes, and androgen receptor (AR) in HNSCC. DNA methylation levels at three CpG sites within the RAD54L2 gene were linked to patient prognosis. Furthermore, RAD54L2 expression was associated with multiple clinicopathological variables, including M, N, and T stages, age, gender, race, tumor status, and overall stage. ROC analysis and nomogram model indicated that RAD54L2 effectively discriminated HNSCC from non-tumor tissues. These findings underscore the potential diagnostic and prognostic utility of RAD54L2, supporting its promise as a therapeutic target in HNSCC.

Keywords: RAD54L2; Head and Neck Squamous Cell Carcinoma; HNSCC; Prognosis

1. Introduction

Head and Neck Squamous Cell Carcinoma (HNSCC) is the sixth most common malignant tumor globally, characterized clinically by strong local invasiveness, high early lymph node metastasis rate, and a tendency to relapse after treatment [1]. Currently, the first-line clinical treatment for HNSCC adopts a comprehensive treatment model primarily based on surgery, radiotherapy, and drug therapy [2, 3]. However, current HNSCC treatment still faces numerous challenges, including treatment resistance, tumor heterogeneity, and treatment-related toxic side effects [4]. Furthermore, the lack of reliable predictive biomarkers also limits the implementation of treatments [5]. This dual challenge of treatment response rates and biomarker reliability urgently necessitates the development of more precise strategies and effective diagnostic biomarkers.

RAD54L2 is an important member of the Swi2/Snf2 ATP-dependent DNA helicase superfamily, specifically

involved in homologous recombination repair (HRR) and double-strand break (DSB) repair processes [6]. This protein is essential for preserving genomic integrity through its facilitation and stabilization of RAD51 nucleoprotein filaments [7]. The highest RAD54L2 expression levels are in lung adenocarcinoma, bladder cancer, and hepatocellular cancer—based on transcriptomic analyses and functional studies that show upregulation of RAD54L2 in tumor tissues compared to normal tissues. Elevated RAD54L2 expression is associated with poor prognosis and may contribute to therapy resistance, particularly to agents targeting topoisomerase II, due to its role in resolving TOP2-DNA adducts and maintaining genome stability [6]. Overexpression of RAD54L2 can enhance DNA repair capacity, thereby promoting tumor cell resistance to radiotherapy and platinum-based chemotherapy [8]. In liver cancer, RAD54L2 significantly promotes the invasive and metastatic abilities of tumor cells by activating the PI3K/AKT/GSK3β signaling pathway [9]. It is particularly noteworthy that the expression patterns of RAD54L2 are significantly associated with the early recurrence risk in HNSCC cancer patients, and they exhibit high-specific expression in cases of oral squamous cell carcinoma [10]. Protein interaction network analysis further demonstrates that key node genes in the RAD54L2 core regulatory network are significantly correlated with sorafenib treatment resistance. Clinical analyses indicate that elevated RAD54L2 expression is significantly correlated with unfavorable outcomes in liver cancer patients, establishing it as an independent predictor of prognosis [11]. Single-cell sequencing studies further reveal that RAD54L2 is specifically highly expressed in tumor stem cell subpopulations, potentially playing a key role in tumor recurrence and treatment resistance [12].

The function of RAD54L2 in HNSCC—particularly regarding immune infiltration, proliferation, epigenetic regulation, and clinical prognosis—remains unclear. To address this, we conducted an integrated bioinformatic investigation leveraging TCGA and GEO datasets to clarify its diagnostic and prognostic significance(**Figure 1**).

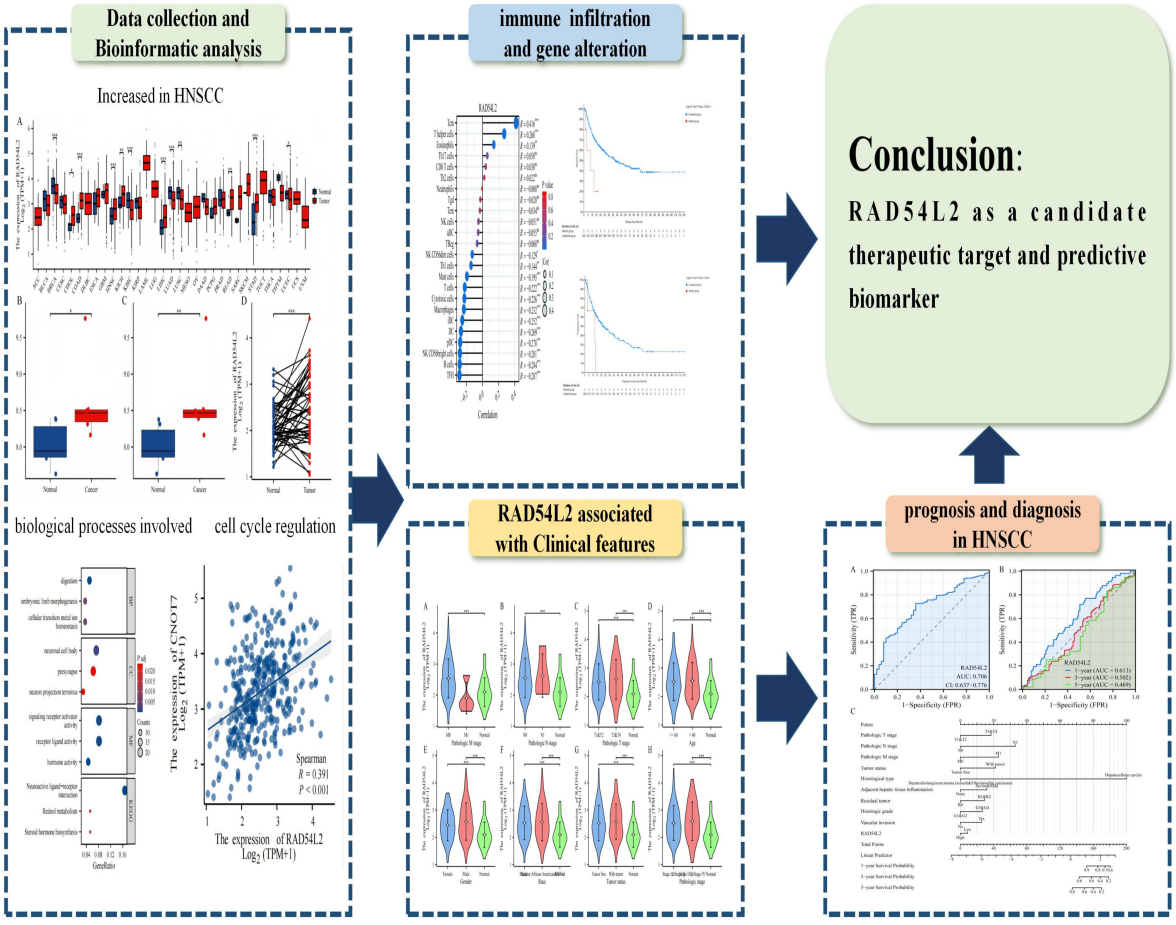

Figure 1. Graphical Abstract.

2. Materials and Methods

2.1. Data Collection

RNA-seq data in FPKM format and matched clinical data from 375 HNSCC cases were acquired from the TCGA-HNSCC project, with expression values converted to TPM. Additionally, two HNSCC datasets (GSE46408, GSE84402) were obtained from GEO. Both repositories are publicly available, and all included patients provided written informed consent.

2.2. Bioinformatics Analysis of RAD54L2 mRNA Expression in HNSCC and Normal Tissues

RAD54L2 mRNA expression profiles were extracted from the TCGA database across 33 cancer types, encompassing 325 HNSCC and 50 normal liver specimens. Supplementary expression data from GEO datasets GSE46408 and GSE84402 were also incorporated. Based on the median expression level, the 375 HNSCC cases were stratified into high- and low-RAD54L2 groups. Differential gene expression between these cohorts was analyzed with the "DESeq2" R package (v1.26.0), applying thresholds of $|\log FC| > 1.5$ and $p < 0.05$. Resulting DEGs were visualized via volcano plots and heatmaps generated using 'ggplot2' (v3.3.3).

2.3. Functional Enrichment Profiling of DEGs Linked to RAD54L2 in HNSCC

Gene symbol conversion from Entrez IDs was performed using the 'org.Hs.eg.db' R package (v3.10.0). Functional annotation and GSEA of DEGs were carried out with 'ClusterProfiler' (v3.14.3), referencing the c2.cp.v7.2.symbols.gmt gene set. Significant enrichment was defined as FDR < 0.25 and adjusted p-value < 0.05. Protein-protein interactions were analyzed via the STRING database and visualized using Cytoscape (v3.9.0).

2.4. Exploring the Correlation between RAD54L2 Expression Levels and the Infiltration of Immune Cells in HNSCC

Employing the ssGSEA algorithm within the 'GSVA' R package (v1.34.0), we quantified the infiltration levels of 24 immune cell subtypes within the tumor microenvironment. These encompassed neutrophils, cytotoxic cells, dendritic cells (DCs), CD8+ T cells, plasmacytoid DCs (pDC), natural killer (NK) cells, mast cells, T gamma delta (Tgd) cells, Th17 cells, immature DCs (iDCs), eosinophils, NK CD56dim cells, regulatory T cells (TReg), effector memory T cells (Tem), T cells, central memory T cells (Tcm), B cells, Th1 cells, macrophages, NK CD56bright cells, activated DCs (aDC), T follicular helper (TFH) cells, T helper cells, and Th2 cells. Subsequently, Spearman's correlation analysis was applied to evaluate associations among RAD54L2 expression, immune infiltration patterns, and specific immune cell markers.

2.5. Correlative Analysis of RAD54L2 Expression Levels, Cell Cycle Modulation, and Hormone Receptors within HNSCC

The relationship between RAD54L2 expression levels, cell cycle regulation genes (CNOT7, NR5A2, DYRK1A, DCAF7, TP53BP1, FAM117B, SQSTM1, and SUMO2), and AR was analyzed in HNSCC samples from the TCGA database using Spearman's correlation analysis with the "ggplot2" (v3.3.3) R package. A correlation was deemed significant if the p-value was less than 0.05.

2.6. Analysis of DNA Methylation Patterns within the CpG Islands of the RAD54L2

The methylation status of specific CpG sites in the RAD54L2 gene was evaluated in HNSCC samples from TCGA via the MethSurv platform to assess its prognostic relevance and association with patient outcomes.

2.7. Genetic Alterations in the HNSCC Samples

The genomic alterations in the *RAD54L2* gene were analyzed using cBioPortal in the following HNSCC datasets: MERiC/Basel, Nat Commun 2022; MSK, 2024; MSK, Clin Cancer Res 2018; INSERM, Nat Genet 2015; MSK, JCO Precis Oncol 2023; MSK, PLOS One 2018; AMC, Hepatology 2014; RIKEN, Nat Genet 2012; and TCGA, PanCancer Atlas. K-M survival curve analysis and log-rank test were conducted to assess the prognostic significance of genomic alterations in the RAD54L2 gene. $p < 0.05$ was considered statistically significant.

2.8. Analysis of the Correlation between RAD54L2 Expression Levels and the Clinicopathological Characteristics of HNSCC Patients

Clinicopathological parameters—including overall survival (OS), disease-specific survival (DSS), progression-free interval (PFI), pathologic T/N/M stages, tumor status, demographic features (gender, race, age, weight, height), and histological subtype—were retrieved from the TCGA-HNSCC cohort. These variables were compared between RAD54L2 high- and low-expression subgroups using R. Normality was evaluated with the Shapiro-Wilk test; group differences for non-normally distributed data were analyzed using the Kruskal-Wallis test followed by Dunn's multiple comparisons, with Bonferroni adjustment for significance thresholds. Results were visualized via 'ggplot2' (v3.3.3), and associations between RAD54L2 expression and clinicopathological features were further examined through logistic regression.

2.9. Assessing the Prognostic Importance of RAD54L2 Expression in HNSCC

Survival analysis of HNSCC patients from TCGA-HNSCC was performed using the 'survival' (v3.2-10) and 'survminer' (v0.4.9) R packages for computation and visualization, respectively. Kaplan-Meier curves along with univariate and multivariate Cox regression, were employed to evaluate the association between RAD54L2 expression and survival outcomes. The diagnostic performance of RAD54L2 was assessed via ROC and time-dependent ROC curves generated with the "pROC" (v1.17.0.1) and "timeROC" (v0.4) packages, while a nomogram was constructed using "ggplot2" (v3.3.3) to visualize predictive accuracy. Subgroup prognostic analysis was further conducted using the K-M methodology. Results are presented with sample size (percentage), hazard ratio (HR), confidence interval (CI), and corresponding *p*-values.

3. Results

3.1. RAD54L2 Expression Levels Are Notably Increased in Diverse Malignancies

RAD54L2 expression was profiled across 33 cancer types within the TCGA database, revealing significant upregulation in 8 tumor types (**Figure 2a**). Among all the cancers analyzed, RAD54L2 was found to be significantly downregulated in four types. Moreover, analysis of the GSE46408 and GSE84402 datasets consistently revealed significantly elevated RAD54L2 expression ($p < 0.05$) in HNSCC tissues (**Figure 2b**,**c**). This upregulation was confirmed by comparing normal tissue specimens (data from GTEx) with adjacent HNSCC tissues and HNSCC tissue specimens (50 pairs, **Figure 2d**).

3.2. Genes with Differential Expression in HNSCC Patients Stratified by High Versus Low RAD54L2 Expression

Based on median RAD54L2 expression, 375 HNSCC cases were stratified into high- and low-expression cohorts. Differential expression analysis identified 674 genes ($|logFC| > 1.5$, $p < 0.05$), with 415 upregulated and 259 downregulated in the high-expression group (**Figure 2e**). A co-expression heatmap of the most significant DEGs is presented in **Figure 2f**.

3.3. Functional Enrichment Analysis of DEGs Linked to RAD54L2 in HNSCC

We conducted a functional annotation of the RAD54L2-associated DEGs in HNSCC patients using the 'clusterProfiler' R package. The results of the GO enrichment analysis are presented in **Figure 3**. The primary biological processes involved were embryonic limb development, digestion, and cellular transition metal ion homeostasis. The most significantly enriched cellular components comprised the neuronal cell body, presynapse, and neuron projection terminus. Molecular functions were predominantly associated with signaling receptor activator activity, receptor ligand activity, and hormone activity. Gene Set Enrichment Analysis (GSEA) indicated that RAD54L2-linked differentially expressed genes were markedly enriched in mitochondrial respiration pathways (**Figure 4a–f**), particularly involving electron transport chain and oxidative phosphorylation systems (NES = −3.248, Padj < 0.001, FDR < 0.001), respiratory electron transport Atp synthesis by chemiosmotic coupling and heat production by uncoupling proteins (NES = −3.092, Padj < 0.001, FDR < 0.001), oxidative phosphorylation (NES = −3.012, Padj < 0.001, FDR < 0.001), respiratory electron transport (NES = −2.974, Padj < 0.001, FDR < 0.001), oxidative phosphorylation (NES = −2.907, Padj < 0.001, FDR < 0.001), the citric acid Tca cycle and respiratory electron transport (NES

= −2.805, Padj < 0.001, FDR < 0.001). DEGs linked to RAD54L2 were further enriched within protein translation-related clusters (**Figure 4g–k**) containing ribosome (NES = −3.073, Padj < 0.001, FDR < 0.001), eukaryotic translation elongation (NES = −3.052, Padj < 0.001, FDR < 0.001), Srp dependent cotranslational protein targeting to membrane (NES = −3.022, Padj < 0.001, FDR < 0.001), response of EIF2AK4 Gcn2 to amino acid deficiency (NES = −3.022, Padj < 0.001, FDR < 0.001), cytoplasmic ribosomal proteins (NES = −2.962, Padj < 0.001, FDR < 0.001). The RAD54L2-associated DEGs exhibited significant correlations with Parkinson's disease, retinoblastoma gene in cancer, Huntington's disease, selenoamino acid metabolism, and nonsense-mediated decay Nmd (**Figure 4l–p**).

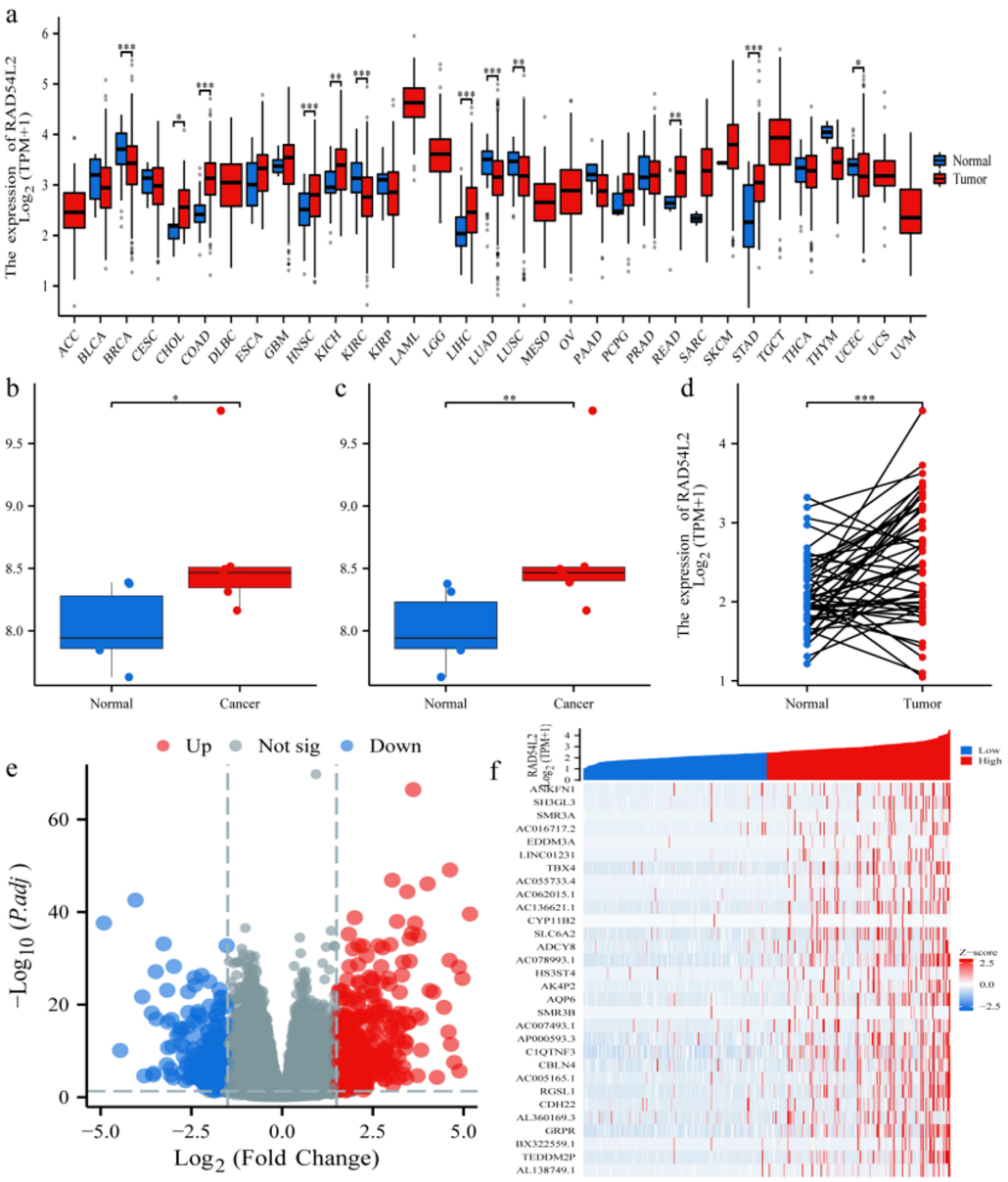

Figure 2. RAD54L2 is significantly upregulated across multiple cancer types, notably in HNSCC. (**a**) Analysis of TCGA data shows RAD54L2 expression in 33 cancers versus adjacent normal tissues. (**b**,**c**) Consistent upregulation of RAD54L2 in HNSCC compared to non-tumor tissues was validated in the GSE46408 and GSE84402 datasets. (**d**) Elevated expression was further confirmed by comparing normal, adjacent non-tumor, and HNSCC tissue samples. (**e**,**f**) Volcano plot and heatmap visualize DEGs between high and low RAD54L2 expression groups in 375 HNSCC patients.

Note: ns, $p \geq 0.05$; *, $p < 0.05$; **, $p < 0.01$; ***, $p < 0.001$.

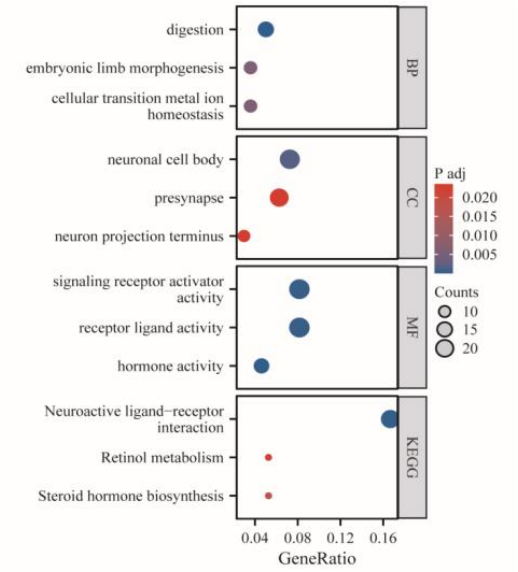

Figure 3. GO enrichment of RAD54L2-associated DEGs.

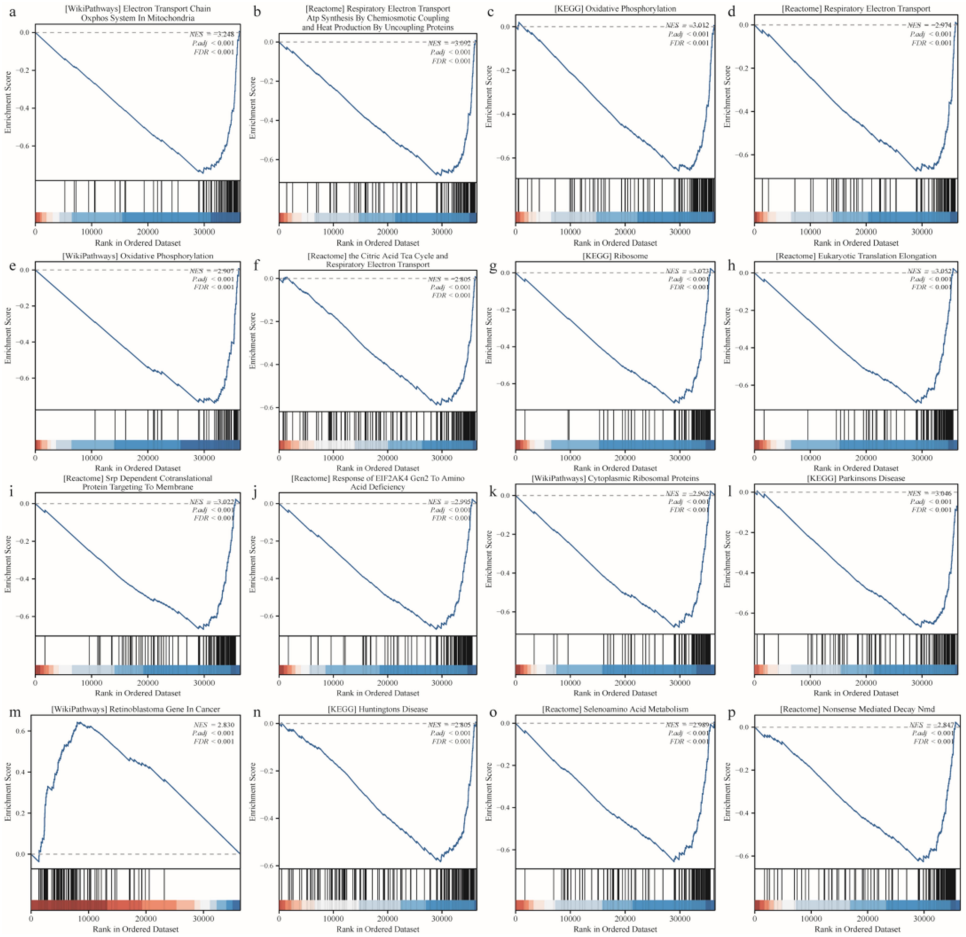

Figure 4. Functional enrichment analysis of DEGs stratified by RAD54L2 expression in HNSCC. (**a–p**) GSEA of altered signaling pathways in HNSCC tissues using DEGs identified between high and low RAD54L2 expression groups.

3.4. RAD54L2 Expression Levels Are Associated with the Infiltration of Various Immune Cell Types

Infiltration levels of 24 immune cell subtypes in HNSCC tissues were evaluated via ssGSEA. Spearman's correlation analysis revealed significant associations between RAD54L2 expression and immune infiltration. Positive correlations were observed with Tcm (R = 0.416, $p < 0.001$), T helper cells (R = 0.268, $p < 0.001$), and eosinophils (R = 0.139, $p < 0.01$). In contrast, negative correlations were identified for TFH (R = −0.287, $p < 0.001$), B cells (R = −0.284, $p < 0.001$), NK CD56bright cells (R = −0.281, $p < 0.001$), dendritic cells (R = −0.269, $p < 0.001$), macrophages (R = −0.232, $p < 0.001$), and cytotoxic cells (R = −0.226, $p < 0.001$) (**Figure 5a**). The infiltration patterns of Tcm and TFH (**Figure 5b**), NK CD56bright and T helper cells (**Figure 5c**), as well as eosinophils and macrophages (**Figure 5d**), were consistent with the correlation trends identified by Spearman's analysis in **Figure 5a**. Additionally, research findings discovered that RAD54L2 expression correlates with markers of various immune cell subpopulations, including TFH, Tcm, and Th1 cells.

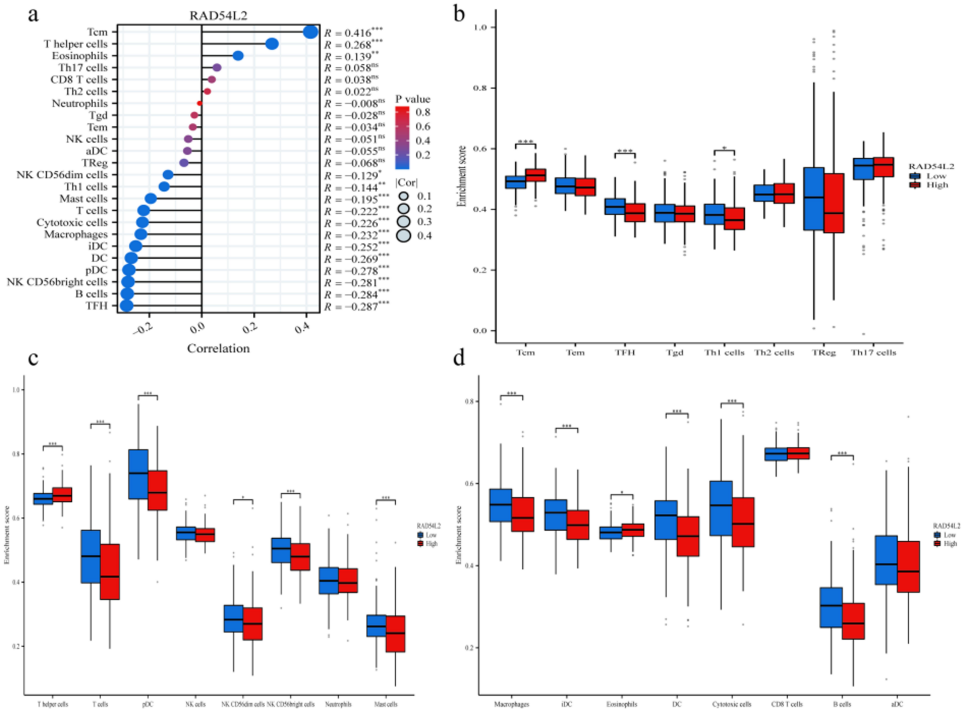

Figure 5. Correlation of immune infiltration with RAD54L2 expression in HNSCC. (**a**) Spearman's correlation between RAD54L2 expression and infiltration abundance of 24 immune cell types. (**b–d**) Infiltration levels and marker expression of selected immune cell subsets in high versus low RAD54L2 expression groups.

3.5. RAD54L2 Expression Levels Are Associated with the Expression of Cell Cycle Regulation Genes and AR in HNSCC

CNOT7, NR5A2, DYRK1A, DCAF7, TP53BP1, FAM117B, SQSTM1, and SUMO2 are key proteins in cell cycle regulation and tumor proliferation. NR3C1 and AR are hormone receptors potentially linked to the inhibition of antitumor immunity. RAD54L2 expression showed significant positive correlations with multiple genes—including CNOT7, NR5A2, DYRK1A, DCAF7, TP53BP1, FAM117B, SQSTM1, SUMO2, NR3C1, and AR—in TCGA HNSCC samples (**Figure 6**).

3.6. Methylation Status of the *RAD54L2* Gene Is Linked to the Prognosis of HNSCC Patients

Using the MethSurv database, DNA methylation patterns and prognostic relevance of CpG sites within the RAD54L2 gene were evaluated. Six methylated CpG islands—including cg16897579, cg02423494, and cg18422423—showed increased methylation levels (**Figure 7**). Additionally, hypermethylation at three specific sites (cg05101231, cg11095658, and cg16897579) was significantly correlated with patient prognosis ($p < 0.05$) (**Table 1**).

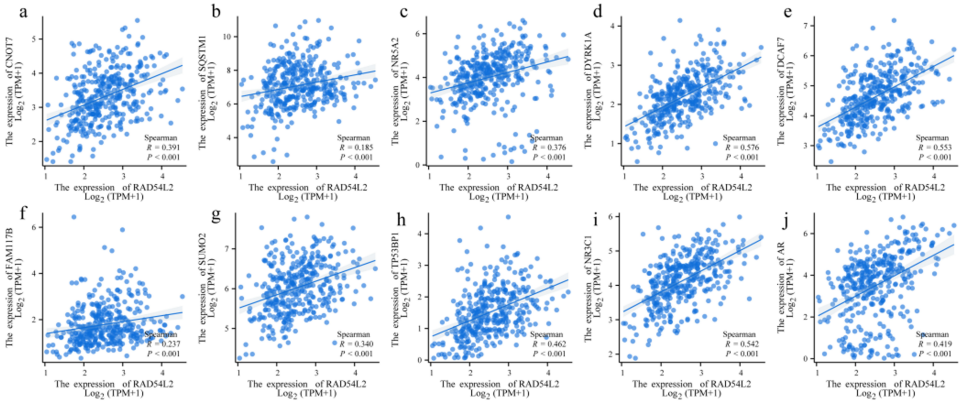

Figure 6. Relation analysis examines the expression levels of RAD54L2, CNOT7, NR5A2, DYRK1A, DCAF7, TP53BP1, FAM117B, SQSTM1, NR3C1, and AR in HNSCC. (**a–j**) Correlation analysis findings regarding the expression levels of RAD54L2 and the subsequent genes in the TCGA-HNSCC dataset: (**a**) CNOT7, (**b**) SQSTM1, (**c**) NR5A2, (**d**) DYRK1A, (**e**) DCAF7, (**f**) FAM117B, (**g**) SUMO2, (**h**) TP53BP1, (**i**) NR3C1, and (**j**) AR.

Figure 7. Methylation levels within the RAD54L2 gene have been linked to the prognosis of individuals with HNSCC.

Table 1. Association between RAD54L2 CpG site methylation and HNSCC prognosis.

Name	HR	*p* value
cg00213142	0.735	0.11
cg02423494	0.796	0.22
cg05101231	1.933	0.00076
cg08030373	1.189	0.4
cg11095658	1.766	0.0016
cg16897579	2.012	0.0041
cg18422423	1.365	0.17
cg20133901	1.297	0.16

3.7. Genetic Changes in RAD54L2 Are Linked to Survival Outcomes in HNSCC Patients

We analyzed genetic alterations in the RAD54L2 gene using samples from HNSCC patients in the following datasets: MERiC/Basel, Nat Commun 2022; MSK 2024; MSK, Clin Cancer Res 2018; INSERM, Nat Genet 2015; MSK, JCO Precis Oncol 2023; MSK, PLOS One 2018; AMC, Hepatology 2014; RIKEN, Nat Genet 2012; TCGA, PanCancer Atlas. Genetic alterations in RAD54L2 were detected in fewer than 1% of HNSCC cases (**Figure 8a**). Kaplan-Meier analysis with log-rank testing revealed significantly worse disease-specific survival (DSS) and progression-free survival (PFS) (both $p < 0.05$) in patients harboring these alterations compared to those without (**Figure 8b,c**).

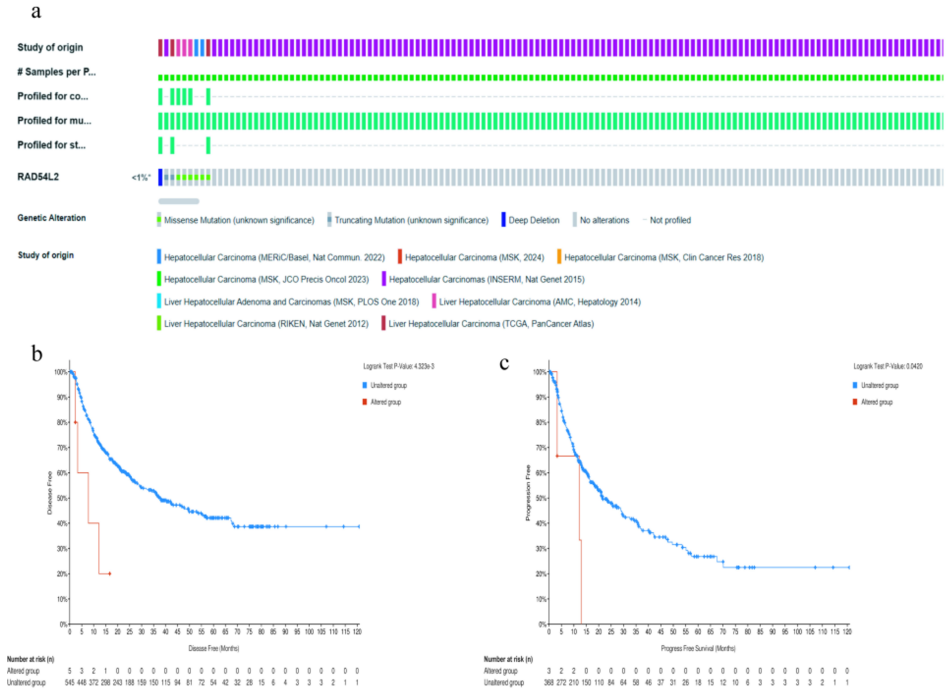

Figure 8. RAD54L2 genetic alterations are associated with survival in HNSCC. (**a**) OncoPrint visualization of RAD54L2 genomic changes. (**b,c**) Kaplan-Meier curves comparing disease-specific survival (**b**) and progression-free survival (**c**) between HNSCC patients with and without RAD54L2 alterations.

3.8. RAD54L2 Expression Levels Are Associated with Various Clinicopathological Features in HNSCC

Based on the TCGA-HNSCC cohort, **Table 2** summarizes the correlations between RAD54L2 expression and clinicopathological features in HNSCC patients. However, there were no significant differences in pathologic T/N/M stages, pathologic stage, tumor status, gender, race, age, weight, height, or histological type among HNSCC patients exhibiting high versus low expression levels of RAD54L2. RAD54L2 expression showed significant associations with multiple clinicopathological parameters, including pathologic M, N, and T stages, age, gender, race, tumor sta-

tus, and overall pathologic stage in HNSCC patients (**Figure 9**). RAD54L2 expression was significantly elevated in Asian patients relative to White patients. Higher expression levels were also observed in patients at pathologic M0 and N0 stages.

Table 2. Clinicopathological features of HNSCC patients with varying RAD54L2 expression levels.

Characteristics	Low Expression of RAD54L2	High Expression of RAD54L2	*p* Value
n	187	187	
Pathologic T stage, n (%)			0.491
T1&T2	143 (38.5%)	135 (36.4%)	
T4&T3	44 (11.9%)	49 (13.2%)	
Pathologic N stage, n (%)			1.000
N0	129 (50%)	125 (48.4%)	
N1	2 (0.8%)	2 (0.8%)	
Pathologic M stage, n (%)			0.646
M0	136 (50%)	132 (48.5%)	
M1	3 (1.1%)	1 (0.4%)	
Pathologic stage, n (%)			0.625
Stage I & Stage II	132 (37.7%)	128 (36.6%)	
Stage III & Stage IV	43 (12.3%)	47 (13.4%)	
Tumor status, n (%)			0.409
Tumor free	104 (29.3%)	98 (27.6%)	
With tumor	72 (20.3%)	81 (22.8%)	
Gender, n (%)			0.581
Female	63 (16.8%)	58 (15.5%)	
Male	124 (33.2%)	129 (34.5%)	
Race, n (%)			0.622
Asian	81 (22.4%)	79 (21.8%)	
White & Black or African American	97 (26.8%)	105 (29%)	
Age, n (%)			0.570
<= 60	91 (24.4%)	86 (23.1%)	
> 60	95 (25.5%)	101 (27.1%)	
Weight, n (%)			0.595
<= 70	89 (25.7%)	95 (27.5%)	
> 70	83 (24%)	79 (22.8%)	
Height, n (%)			0.309
< 170	106 (31.1%)	95 (27.9%)	
>= 170	66 (19.4%)	74 (21.7%)	
Histological type, n (%)			0.200
Head and Neck Squamous Cell Carcinoma	187 (50.0%)	187 (50.0%)	

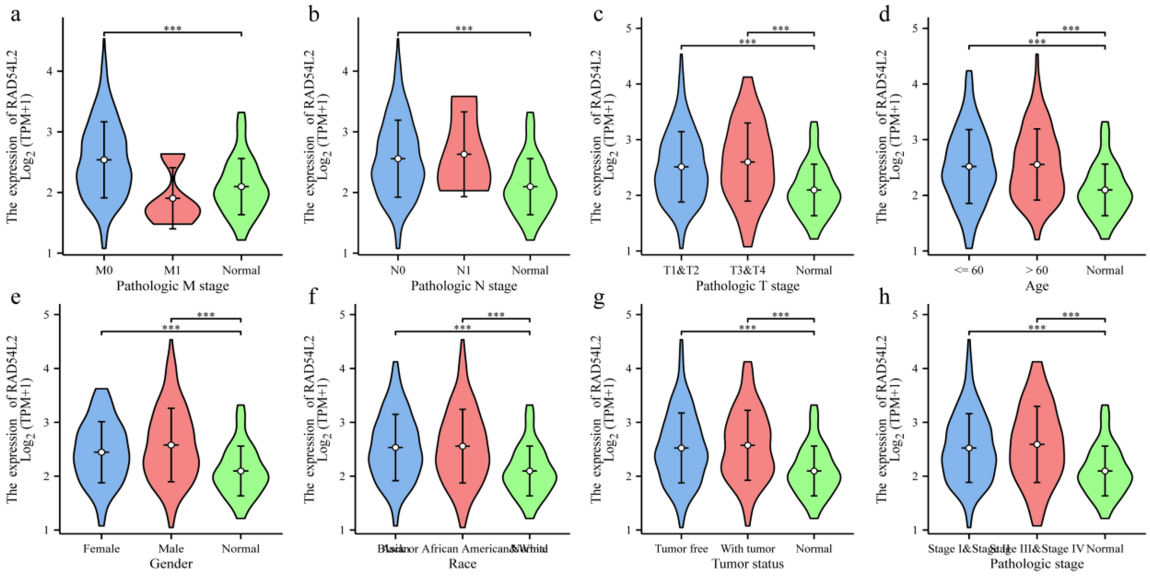

Figure 9. RAD54L2 expression is correlated with diverse clinicopathological characteristics in HNSCC patients. (**a–h**) Associations between RAD54L2 expression and (**a**) M stage, (**b**) N stage, (**c**) T stage, (**d**) age, (**e**) gender, (**f**) race, (**g**) tumor status, and (**h**) overall pathologic stage.

Note: ***$p < 0.001$.

3.9. RAD54L2 Shows Promise as a Potential Biomarker for Both Prognosis and Diagnosis in HNSCC

Survival analysis revealed that HNSCC patients exhibiting high RAD54L2 expression experienced reduced overall survival (OS, $p > 0.05$; **Figure 10a**), disease-specific survival (DSS, $p > 0.05$; **Figure 10b**), and progression-free interval (PFI, $p > 0.05$; **Figure 10c**) relative to the low-expression group. Multivariate Cox regression demonstrated that RAD54L2 was not an independent prognostic factor for OS, DSS, or PFI (**Tables 3–5**). Pathologic T stage emerged as an independent predictor for both OS (**Table 3**) and PFI (**Table 5**), while tumor status independently predicted OS (**Table 3**) and DSS (**Table 4**). Additionally, vascular invasion was significantly associated with DSS (**Table 4**).

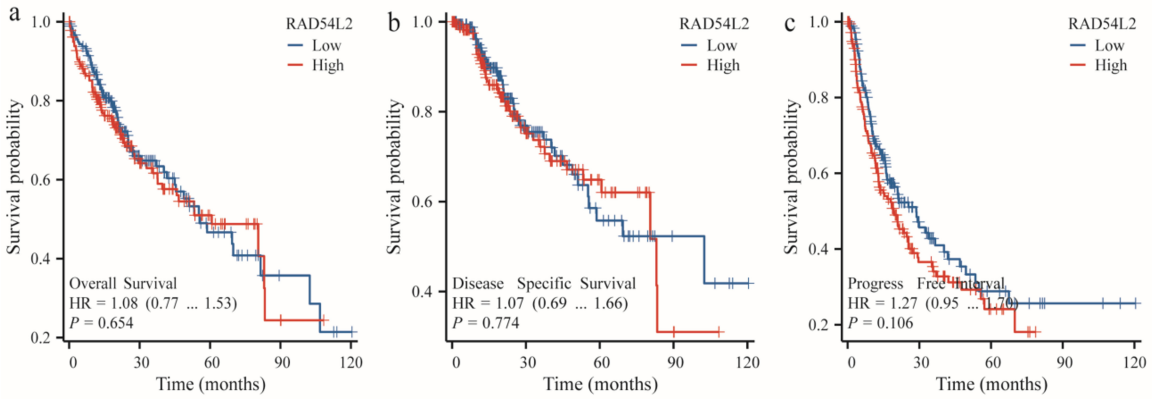

Figure 10. Prognostic significance of RAD54L2 in HNSCC. Analysis using the Kaplan-Meier plotter revealed no statistically significant differences in (**a**) overall survival (OS), (**b**) disease-specific survival (DSS), or (**c**) progression-free interval (PFI) between patients with high versus low RAD54L2 expression ($p < 0.05$ considered significant).
Note: High and low expression groups are represented by red and blue curves, respectively.

Table 3. Cox regression analysis of the OS in HNSCC patients based on various clinicopathological characteristics.

Characteristics	Total (N)	Univariate Analysis		Multivariate Analysis	
		Hazard Ratio (95% CI)	*p* Value	Hazard Ratio (95% CI)	*p* Value
Pathologic T stage	370				
T1&T2	277	Reference		Reference	
T3&T4	93	2.598 (1.826–3.697)	<0.001	2.413 (1.533–3.798)	<0.001
Pathologic N stage	258				
N0	254	Reference			
N1	4	2.029 (0.497–8.281)	0.324		
Pathologic M stage	272				
M0	268	Reference		Reference	
M1	4	4.077 (1.281–12.973)	0.017	1.285 (0.306–5.400)	0.732
Tumor status	354				
Tumor free	202	Reference		Reference	
With tumor	152	2.317 (1.590–3.376)	<0.001	2.024 (1.272–3.220)	0.003
Histological type	373	0.439 (0.061–3.145)	0.412		
Adjacent tissue inflammation	236				
None	118	Reference			
Severe&Mild	118	1.194 (0.734–1.942)	0.475		
Residual tumor	344				
R0	326	Reference			
R1&R2	18	1.604 (0.812–3.169)	0.174		
Histologic grade	368				
G1&G2	233	Reference			
G3&G4	135	1.091 (0.761–1.564)	0.636		
Vascular invasion	317				
No	208	Reference			
Yes	109	1.344 (0.887–2.035)	0.163		
RAD54L2	373				
Low	186	Reference			
High	187	1.082 (0.766–1.528)	0.654		

Table 4. Cox proportional hazards regression for DSS in HNSCC patients using multiple clinicopathological variables.

Characteristics	Total (N)	Univariate Analysis		Multivariate Analysis	
		Hazard Ratio (95% CI)	*p* Value	Hazard Ratio (95% CI)	*p* Value
Pathologic T stage	370				
T1&T2	277	Reference		Reference	
T3&T4	93	2.177 (1.590–2.980)	<0.001	1.414 (0.875–2.287)	0.157
Pathologic N stage	258				
N0	254	Reference			
N1	4	1.370 (0.338–5.552)	0.659		
Pathologic M stage	272				
M0	268	Reference		Reference	
M1	4	3.476 (1.091–11.076)	0.035	1.884 (0.559–6.350)	0.307
Tumor status	354				
Tumor free	202	Reference		Reference	
With tumor	152	11.342 (7.567–17.000)	<0.001	14.584 (8.615–24.689)	<0.001
Histological type	373	1.320 (0.489–3.560)	0.584		
Adjacent tissue inflammation	236				
None	118	Reference			
Severe&Mild	118	1.238 (0.867–1.768)	0.241		
Residual tumor	344				
R0	326	Reference			
R1&R2	18	1.513 (0.840–2.726)	0.168		
Histologic grade	368				
G1&G2	233	Reference			
G3&G4	135	1.152 (0.853–1.557)	0.355		
Vascular invasion	317				
No	208	Reference		Reference	
Yes	109	1.676 (1.196–2.348)	0.003	1.529 (1.004–2.326)	0.048
RAD54L2	373				
Low	186	Reference			
High	187	1.271 (0.950–1.700)	0.106		

Table 5. Cox regression-based analysis of PFI in individuals with HNSCC, incorporating a range of clinicopathological traits.

Characteristics	Total (N)	Univariate Analysis		Multivariate Analysis	
		Hazard Ratio (95% CI)	*p* Value	Hazard Ratio (95% CI)	*p* Value
Pathologic T stage	362				
T1&T2	272	Reference		Reference	
T3&T4	90	3.639 (2.328–5.688)	<0.001	2.595 (1.448–4.653)	0.001
Pathologic N stage	253				
N0	249	Reference			
N1	4	3.612 (0.870–14.991)	0.077		
Pathologic M stage	268				
M0	265	Reference		Reference	
M1	3	5.166 (1.246–21.430)	0.024	1.183 (0.277–5.058)	0.820
Tumor status	354				
Tumor free	202	Reference		Reference	
With tumor	152	775790759.3892 (0.000–Inf)	0.994	921084188.8869 (0.000–Inf)	0.996
Histological type	365	0.000 (0.000–Inf)	0.995		
Adjacent tissue inflammation	232				
None	115	Reference			
Severe & Mild	117	1.403 (0.768–2.566)	0.271		
Residual tumor	337				
R0	320	Reference			
R1&R2	17	1.678 (0.728–3.870)	0.224		
Histologic grade	360				
G1&G2	227	Reference			
G3&G4	133	1.086 (0.683–1.728)	0.726		
Vascular invasion	309				
No	204	Reference			
Yes	105	1.277 (0.707–2.306)	0.418		
RAD54L2	365				
Low	182	Reference			
High	183	1.067 (0.685–1.661)	0.774		

ROC analysis was performed to evaluate the diagnostic performance of RAD54L2 expression, which effectively distinguished tumors from adjacent non-tumor tissues with an AUC of 0.706 (**Figure 11a**). Time-dependent ROC

curves indicated AUC values exceeding 0.5 for predicting 1- and 3-year survival in HNSCC patients using RAD54L2 expression (**Figure 11b**). A nomogram integrating pathologic T/N/M stage, tumor status, histologic type, adjacent hepatic tissue inflammation, residual tumor, histologic grade, vascular invasion, and RAD54L2 expression was constructed. This model showed significant predictive accuracy for 1-, 3-, and 5-year survival probabilities (**Figure 11c**).

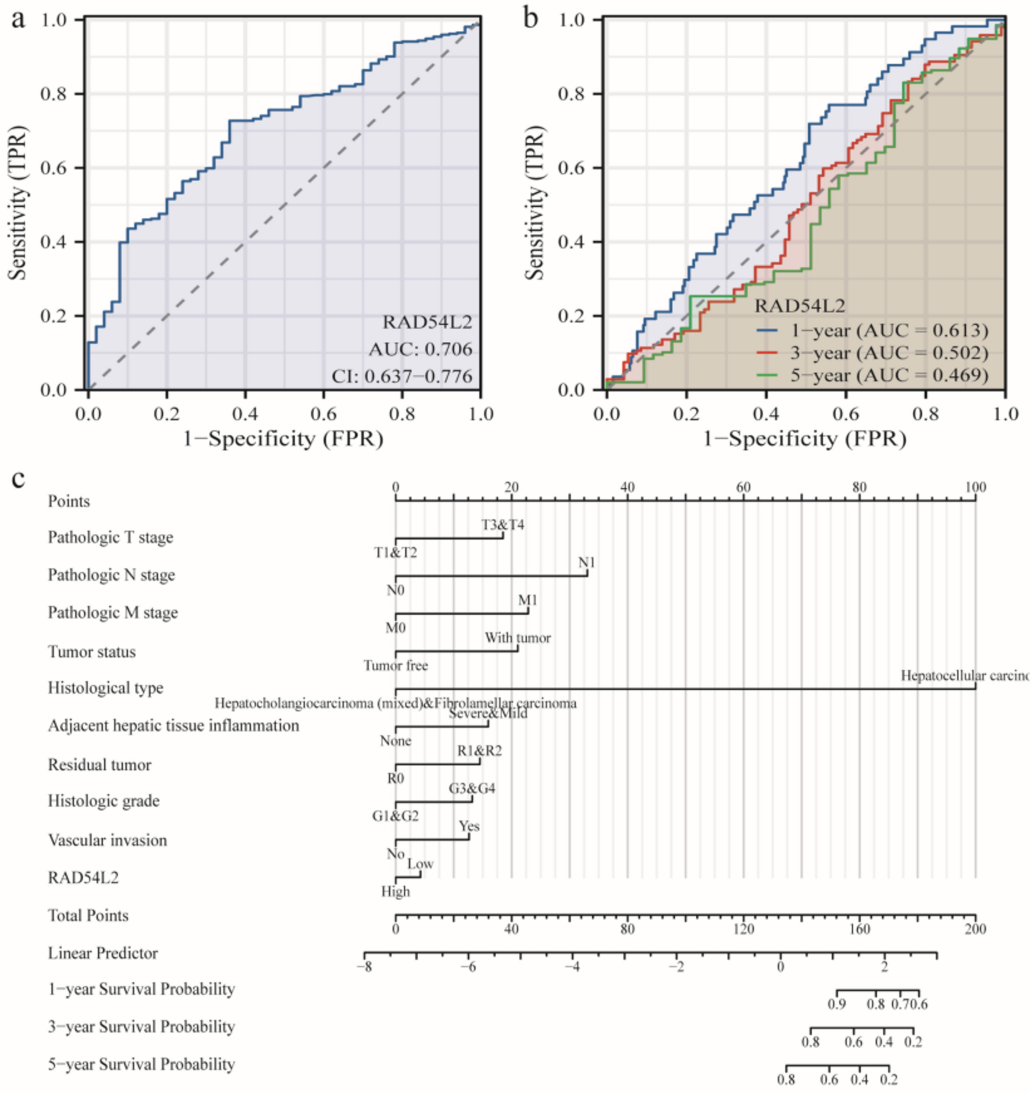

Figure 11. A nomogram integrating RAD54L2 demonstrates improved diagnostic and prognostic performance in HNSCC. (**a**) Diagnostic ROC curve distinguishing HNSCC from non-tumor tissues using RAD54L2. (**b**) Time-dependent ROC analysis predicting 1-, 3-, and 5-year survival based on RAD54L2 expression. (**c**) ROC evaluation of the nomogram's predictive accuracy for 1-, 3-, and 5-year survival, incorporating clinicopathological variables and RAD54L2 expression.

3.10. The Prognostic Performance of RAD54L2 in Various Clinicopathological Subgroups of HNSCC

Table 6 summarizes Cox regression results evaluating the prognostic significance of RAD54L2 across specific HNSCC patient subgroups stratified by clinicopathological features. HNSCC patients with certain clinicopathological parameters, particularly pathologic T3 and T4 stages ($p < 0.001$), and the presence of tumors ($p = 0.003$), were associated with unfavorable clinical outcomes.

Table 6. Prognostic value of RAD54L2 across HNSCC patient subgroups via Cox regression analysis.

Characteristics	Total (N)	HR (95% CI Univariate Analysis)	P Value Univariateanalysis	HR (95% CI) Multivariate Analysis	*p* Value Multivariate Analysis
Pathologic T stage	370				
T1&T2	277	Reference		Reference	
T3&T4	93	2.598 (1.826–3.697)	< 0.001	2.413 (1.533–3.798)	< 0.001
Pathologic N stage	258				
N0	254	Reference			
N1	4	2.029 (0.497–8.281)	0.324		
Pathologic M stage	272				
M0	268	Reference		Reference	
M1	4	4.077 (1.281–12.973)	0.017	1.285 (0.306–5.400)	0.732
Tumor status	354				
Tumor free	202	Reference		Reference	
With tumor	152	2.317 (1.590–3.376)	< 0.001	2.024 (1.272–3.220)	0.003
Histological type	373	0.439 (0.061–3.145)	0.412		
Adjacent tissue inflammation	236				
None	118	Reference			
Severe & Mild	118	1.194 (0.734–1.942)	0.475		
Residual tumor	344				
R0	326	Reference			
R1&R2	18	1.604 (0.812–3.169)	0.174		
Histologic grade	368				
G1&G2	233	Reference			
G3&G4	135	1.091 (0.761–1.564)	0.636		
Vascular invasion	317				
No	208	Reference			
Yes	109	1.344 (0.887–2.035)	0.163		
RAD54L2	373				
Low	186	Reference			
High	187	1.082 (0.766–1.528)	0.654		

4. Discussion

In this study, we found that RAD54L2 was significantly overexpressed in many human cancer tissues, and high expression was observed in HNSCC tissues from clinical samples as well as the TCGA and GEO databases, indicating that RAD54L2 may be a potential biomarker for HNSCC.

At the molecular level, overexpression of RAD54L2 not only enhances homologous recombination repair efficiency but also abnormally activates the replication fork protection mechanism, leading to significant genomic stability advantages for tumor cells [13]. DEGs significantly associated with RAD54L2 are mainly enriched in three core biological processes: mitotic spindle assembly checkpoint, hypoxia stress response, and mitochondrial electron transport chain complex assembly [14]. Single-cell ATAC-seq data confirms that cells with high RAD54L2 expression exhibit unique chromatin accessibility features, particularly at sites associated with stem cell properties, which may serve as the epigenetic basis for promoting tumor heterogeneity [15]. These findings systematically elucidate the mechanisms by which RAD54L2 drives the malignant progression of cancer through a multidimensional regulatory network.

Research indicates that inflammation-related biomarkers are significantly upregulated in liver cancer tissues, promoting the formation of an immunosuppressive microenvironment [16]. Our findings suggest a potential link between RAD54L2 expression and immune infiltration in hepatocellular carcinoma. Specifically, RAD54L2 levels show negative correlations with the abundance of TFH cells, B cells, NK CD56bright cells, dendritic cells, cytotoxic cells, and macrophages. Among them, TFH influences anti-tumor immunity by regulating B cell antibody responses [17]. The infiltration of B cells into tumors is associated with better prognosis, possibly enhancing anti-tumor responses through antigen presentation and immunoregulatory functions [18]. NK CD56bright cells have a stronger ability to secrete cytokines, which enhances the antigen-presenting function of dendritic cells (DCs) [19]. Additionally, the infiltration of cytotoxic T cells and M1-type macrophages is related to tumor suppression, whereas M2-type macrophages promote immune escape [20]. Our results indicated a positive association between RAD54L2 expression and infiltration levels of Tcm, T helper cells, and eosinophils in hepatocellular carcinoma. These immune cell subtypes—Tcm, Th, and eosinophils—are critically involved in mediating anti-tumor immune responses. Tcm cells, due to their long-term survival capability and rapid effector functions, demonstrate sustained anti-tumor activity in liver cancer immunotherapy [21]. Th cells regulate the tumor microenvironment by secreting cytokines such as IL-4 and IL-5. Th1 cells promote anti-tumor immunity, while Th2 cells may inhibit

immune responses [22]. Notably, eosinophils activate CD8+ T cells and enhance anti-tumor effects by releasing granule proteins (such as ECP, MBP) and cytokines (IL-5, GM-CSF) [23]. Single-cell sequencing analysis reveals that the infiltration levels of Tcm and Th cells in liver cancer tissues are positively correlated with patient overall survival (HR = 0.62, 95% CI 0.48–0.80) [24]. Additionally, eosinophils can limit tumor progression by inducing tumor cell apoptosis and inhibiting angiogenesis [25]. Elevated RAD54L2 expression may facilitate immune evasion in Head and Neck Squamous Cell Carcinoma, potentially supporting tumor growth and disease progression.

This study thoroughly examines the intricate regulatory network of several key genes, including CNOT7, NR5A2, DYRK1A, DCAF7, TP53BP1, FAM117B, SQSTM1, SUMO2, and AR, in the development and progression of liver cancer. CNOT7, as a core component of the mRNA degradation complex, promotes tumor progression by selectively degrading the mRNA of tumor suppressor genes [26]. NR5A2, as a key transcription factor in metabolic regulation, promotes the maintenance of liver cancer cell stemness and chemoresistance by reprogramming fatty acid metabolism [27]. The DYRK1A-DCAF7 complex not only activates the Wnt pathway through stabilizing β-catenin but also phosphorylates p53 to regulate its stability [28]. The crucial role of TP53BP1 in DNA damage repair has been widely recognized, and recent studies have found that its deficiency can lead to defects in non-homologous end joining repair and genomic instability [29]. FAM117B acts as a novel regulatory factor of the ERK signaling pathway, promoting tumor metastasis by affecting the EMT process [30]. The selective autophagy system composed of SQSTM1 (p62) and SUMO2 plays a crucial role in maintaining protein homeostasis in tumor cells, with its abnormal expression significantly associated with poor prognosis in liver cancer [29,30]. The sex-specific expression pattern of the androgen receptor (AR) provides a molecular basis for explaining the gender disparity in head and neck squamous cell cancer incidence [31]. Our research shows that RAD54L2 expression levels in HNSCC tissues are positively correlated with those of CNOT7, NR5A2, DYRK1A, DCAF7, TP53BP1, FAM117B, SQSTM1, SUMO2, and AR. This suggests that RAD54L2 could be a potential target for enhancing treatment outcomes in head and neck squamous cell cancer patients.

DNA methylation plays a crucial role in the occurrence and development of head and neck squamous cell carcinoma. There are genome-wide aberrations in DNA methylation in HNSCC, primarily characterized by global hypomethylation and hypermethylation in specific gene promoter regions. These abnormal methylation patterns promote tumorigenesis and tumor progression by affecting the expression of key tumor suppressor genes. Notably, HPV-positive and HPV-negative HNSCC exhibit significantly distinct DNA methylation profiles [32]. This aberrant methylation promotes tumorigenesis by silencing tumor suppressor genes (e.g., RASSF1A, CDKN2A) and activating oncogenes (e.g., c-Myc) [33]. This study examined the association between RAD54L2 methylation status and HNSCC patient outcomes. cg05101231, cg11095658, and cg16897579 were associated with poor prognosis, while cg16897579, cg02423494, and cg18422423 sites showed the highest degree of DNA methylation. TP53, CTNNB1, and TERT promoter mutations represent the most frequently observed driver alterations in HNSCC, promoting tumor progression by affecting cell cycle regulation, Wnt signaling pathway, and telomere maintenance [34]. Notably, methylation markers such as HOXA9 and mutation profiles in circulating tumor DNA (ctDNA) have shown good diagnostic value and provide a basis for targeted treatment selection [35]. Our study revealed that mutations in the RAD54L2 gene occur in less than 1% of HNSCC tissues and are linked to patient PFS and DSS.

Our results demonstrate that RAD54L2 expression in HNSCC tissues shows significant associations with multiple clinicopathological parameters—including pathological T, N, and M stages; overall pathological stage; tumor status; demographic characteristics (gender, race, age, weight, height); and histological subtype—when compared to normal controls. Additionally, Asian populations have higher RAD54L2 levels than Caucasian populations. Logistic regression revealed positive correlations between RAD54L2 expression in HNSCC and pathological T/N stage, overall pathological stage, tumor status, gender, race, age, and height. Conversely, Kaplan-Meier analysis indicated no significant differences in OS, DSS, or PFI between high and low RAD54L2 expression groups. The area under the curve (AUC) for using RAD54L2 expression levels in diagnosing HNSCC is 0.706. Additionally, the AUC values for predicting one-year and three-year survival rates are both above 0.5. These findings indicate that RAD54L2 could serve as a potential diagnostic and prognostic biomarker in HNSCC. A nomogram incorporating multivariate Cox regression results demonstrated that RAD54L2 expression significantly improves prognostic prediction for HNSCC patients.

Patients with gastric cancer who exhibit high expression of RAD54L2 have significantly shorter overall survival and a higher risk of lymph node metastasis [36]. In breast cancer studies, patients with overexpression of RAD54L2 show

a 38% lower response rate to neoadjuvant chemotherapy, with its predictive value being more pronounced in triple-negative breast cancer [37]. In non-small cell lung cancer, RAD54L2 expression shows a positive correlation with tumor mutational burden and may function as a predictor for immunotherapy response [38]. Among glioblastoma patients, elevated RAD54L2 levels are linked to increased cancer stem cell properties and reduced progression-free survival [39]. Notably, in colorectal cancer, RAD54L2 expression levels are significantly correlated with microsatellite instability status (MSI-H), suggesting its specific role in DNA mismatch repair-deficient tumors [40]. Studies have also found that the RAD54L2 gene is significantly associated with nasopharyngeal cancer susceptibility [41]. These findings indicate that RAD54L2 may serve as a universal prognostic marker and therapeutic target across different tumor types [42].

This study has several limitations. The findings are derived primarily from RNA-seq data of HNSCC tissues obtained from public databases such as TCGA and GEO. Consequently, the activity and protein-level interactions of signaling pathways upstream and downstream of RAD54L2 could not be directly evaluated. Further experimental validation using in vivo and in vitro models is warranted to elucidate the functional mechanisms of RAD54L2 in head and neck squamous cell carcinoma.

5. Conclusions

This study confirms the diagnostic and prognostic relevance of RAD54L2 in head and neck squamous cell carcinoma. RAD54L2 was upregulated in tumor tissues and appears to promote HNSCC progression through modulation of cell cycle and immune-related genes. Its expression correlated with altered infiltration of multiple immune cell types, indicating a possible influence on immunotherapy efficacy. Furthermore, both methylation status and genetic alterations of RAD54L2 were associated with patient prognosis. Besides, RAD54L2 has certain diagnostic and survival prediction capabilities. These results position RAD54L2 as a candidate therapeutic target and predictive biomarker, though additional experimental studies are required for further validation.

Author Contributions

All members of this article participated in the first draft of the article. X.X. is responsible for most of the writing of the article and the experimental data visualization, L.M. is responsible for the data analysis, and the supervision of the experiment. Both authors have read and agreed to the published version of the manuscript.

Funding

This work was supported by a specialized scientific research fund project for clinical medicine of Nantong University [grant number: 2024JQ018].

Institutional Review Board Statement

Not applicable.

Informed Consent Statement

Not applicable.

Data Availability Statement

The data utilized in this study are accessible through online repositories. Details regarding the specific repository names and corresponding accession numbers are provided within the article.

Conflicts of Interest

The authors declare that they have no competing interests.

References

1. Johnson, D.E.; Burtness, B.; Leemans, C.R.; et al. Head and neck squamous cell carcinoma. *Nat. Rev. Dis. Primers* **2020**, *6*, 1–22. [CrossRef]

2. Ferris, R.L.; Blumenschein, G.J.; Fayette, J.; et al. Nivolumab for recurrent squamous-cell carcinoma of the head and neck. *N. Engl. J. Med.* **2022**, *375*, 1856–1867. [CrossRef]
3. Burtness, B.; Harrington, K.J.; Greil, R.; et al. Pembrolizumab alone or with chemotherapy versus cetuximab with chemotherapy for recurrent or metastatic squamous cell carcinoma of the head and neck (KEYNOTE-048): a randomised, open-label, phase 3 study. *Lancet* **2019**, *394*, 1915–1928. [CrossRef]
4. Cramer, J.D.; Burtness, B.; Ferris, R.L. Immunotherapy for head and neck cancer: Recent advances and future directions. *Oral Oncol.* **2019**, *99*, 104460. [CrossRef]
5. Schoenfeld, J.D.; Hanna, G.J.; Jo, V.Y.; et al. Neoadjuvant Nivolumab or Nivolumab plus Ipilimumab in untreated oral cavity squamous cell carcinoma: A phase 2 open-label randomized clinical trial. *JAMA Oncol.* **2020**, *6*, 1563–1570. [CrossRef]
6. D'Alessandro, G.; Morales-Juarez, D.A.; Richards, S.L.; et al. RAD54L2 counters TOP2-DNA adducts to promote genome stability. *Sci. Adv.* **2023**, *9*, eadl2108. [CrossRef]
7. Jung, J.H.; Edith, C.; Cassandra, J.W.; et al. The BLM-TOP3A-RMI1-RMI2 proximity map reveals that RAD54L2 suppresses sister chromatid exchanges. *EMBO. Rep.* **2025**, *26*, 1290–1314. [CrossRef]
8. Diego, D.; Martin, L.; Francesca, V.; et al. H2AX promotes replication fork degradation and chemosensitivity in BRCA-deficient tumours. *Nat. Commun.* **2024**, *15*, 4430. [CrossRef]
9. Gu, Y.; Chen, B.Y.; Guo, D.L.; et al. Up-Regulation of RACGAP1 Promotes Progressions of Hepatocellular Carcinoma Regulated by GABPA via PI3K/AKT Pathway. *Oxid. Med. Cell. Longev.* **2022**, *72*, 3034150. [CrossRef]
10. Cao, X.; Chen, J.L.; Zhang, R.; et al. Study on the expression and function of RAD54L in oral squamous cell carcinoma. *J. Prev. Treat. Stomatol. Dis.* **2024**, *32*, 853–862. [CrossRef]
11. Yuan, J.S.; Lv, T.; Yang, J.; et al. HDLBP Promotes Hepatocellular Carcinoma Proliferation and Sorafenib Resistance by Suppressing Trim71-dependent RAF1 Degradation. *Cell. Mol. Gastroenterol. Hepatol.* **2023**, *15*, 307–325. [CrossRef]
12. Liu, H.; Sima, X.X; Xiao, B.J.; et al. Integrated analysis of single-cell and bulk RNA sequencing data reveals a myeloid cell-related regulon predicting neoadjuvant immunotherapy response across cancers. *J. Transl. Med.* **2024**, *22*, 486. [CrossRef]
13. Wu, W.J.; Wu, W.J.; Xie, X.X.; et al. DNMT1 is required for efficient DSB repair and maintenance of replication fork stability, and its loss reverses resistance to PARP inhibitors in cancer cells. *Oncogene* **2025**, 44, 2283–2302. [CrossRef]
14. Verma, S.; Sahu, B.D.; Mugale, M.N. Role of lncRNAs in hepatocellular carcinoma. *Life. Sci.* **2023**, *325*, 121751. [CrossRef]
15. Wang, C.Q.; Huang, W.D.; Zhong, Y.; et al. Single-cell multi-modal chromatin profiles revealing epigenetic regulations of cells in hepatocellular carcinoma. *Clin. Transl. Med.* **2024**, *14*, e7000. [CrossRef]
16. Sun, Y.; Chen, S.; Lu, Y.; et al. Single-cell transcriptomic analyses of tumor microenvironment and molecular reprograming landscape of metastatic laryngeal squamous cell carcinoma. *Commun. Biol.* **2024**, *7*, 63. [CrossRef]
17. Cui, C.; Wang, J.W.; Fagerberg, E.; et al. Neoantigen-driven B cell and CD4 T follicular helper cell collaboration promotes anti-tumor CD8 T cell responses. *Cell* **2021**, *184*, 6101–6118. [CrossRef]
18. Wu, J.X.; Wang, Y.; Bai, S.H.; et al. Aberrant alteration of peripheral B lymphocyte subsets in hepatocellular carcinoma patients. *Int. J. Med. Sci.* **2023**, *20*, 267–277. [CrossRef]
19. Anguille, S.; Acker, H.H.A.; Bergh, J.V.D.; et al. Interleukin-15 Dendritic Cells Harness NK Cell Cytotoxic Effector Function in a Contact- and IL-15-Dependent Manner. *PLoS One* **2015**, *10*, e0123340. [CrossRef]
20. Han, S.L.; Bao, X.Y.; Zou, Y.F.; et al. d-lactate modulates M2 tumor-associated macrophages and remodels immunosuppressive tumor microenvironment for hepatocellular carcinoma. *Sci. Adv.* **2023**, *9*, eadg2697. [CrossRef]
21. Chen, H.; Li, Z.L.; Qiu, L.M.; et al. Personalized neoantigen vaccine combined with PD-1 blockade increases CD8+ tissue-resident memory T-cell infiltration in preclinical hepatocellular carcinoma models. *J. Immunother. Cancer.* **2022**, *10*, e004389. [CrossRef]
22. Vo, M.C.; Jung, S.H.; Chu, T.C.; et al. Lenalidomide and Programmed Death-1 Blockade Synergistically Enhances the Effects of Dendritic Cell Vaccination in a Model of Murine Myeloma. *Front. Immunol.* **2018**, *9*, 1370. [CrossRef]
23. Tal, S.G.; Dulberg, S.; Beck, L.; et al. Metastasis-Entrained Eosinophils Enhance Lymphocyte-Mediated Antitumor Immunity. *Cancer Res.* **2021**, *81*, 5555–5571. [CrossRef]
24. Li, M.Y.; Wang, L.N.; Cong, L.; et al. Spatial proteomics of immune microenvironment in nonalcoholic steatohepatitis-associated hepatocellular carcinoma. *Hepatology* **2024**, *79*, 560–574. [CrossRef]

25. Gambardella, A.R.; Antonucci, C.; Zanetti, C.; et al. IL-33 stimulates the anticancer activities of eosinophils through extracellular vesicle-driven reprogramming of tumor cells. *J. Exp. Clin. Cancer. Res.* **2024**, *43*, 209. [CrossRef]
26. Mishima, Y.; Tomari, Y. Pervasive yet nonuniform contributions of Dcp2 and Cnot7 to maternal mRNA clearance in zebrafish. *Genes Cells* **2017**, *22*, 670–678. [CrossRef]
27. Michalek, S.; Brunner, T. Nuclear-mitochondrial crosstalk: On the role of the nuclear receptor liver receptor homolog-1 (NR5A2) in the regulation of mitochondrial metabolism, cell survival, and cancer. *IUBMB Life* **2021**, *73*, 592–610. [CrossRef]
28. Ansari, A.; Szczesnowska, A.; Haddad, N.; et al. The Role of Non-Coding RNAs in the Regulation of Oncogenic Pathways in Breast and Gynaecological Cancers. *Noncoding RNA* **2025**, *11*, 61. [CrossRef]
29. Ye, Q.; Ma, J.; Wang, Z.X.; et al. DTX3L-mediated TIRR nuclear export and degradation regulates DNA repair pathway choice and PARP inhibitor sensitivity. *Nat. Commun.* **2024**, *15*, 10596. [CrossRef]
30. Zhou, Y.J.; Chen, Y.X.; Shi, Y.W.; et al. FAM117B promotes gastric cancer growth and drug resistance by targeting the KEAP1/NRF2 signaling pathway. *J. Clin. Invest.* **2023**, *133*, e158705. [CrossRef]
31. Tao, X.R.; Wang, Y.L.; Xiang, B.H.; et al. Sex bias in tumor immunity: insights from immune cells. *Theranostics* **2025**, *15*, 5045–5072. [CrossRef]
32. Lechner, M.; Fenton, T.; West, J.; et al. Identification and functional validation of HPV-mediated hypermethylation in head and neck squamous cell carcinoma. *Genome Med.* **2013**, *5*, 15. [CrossRef]
33. Deng, Y.L.; Lu, L.Q.; Liang, X.J.; et al. DNA methylation-mediated silencing of Neuronatin promotes hepatocellular carcinoma proliferation through the PI3K-Akt signaling pathway. *Life. Sci.* **2023**, *312*, 121266. [CrossRef]
34. Caswell, D.R.; Gui, P.; Mayekar, M.K.; et al. The role of APOBEC3B in lung tumor evolution and targeted cancer therapy resistance. *Nat. Genet.* **2024**, *56*, 60–73. [CrossRef]
35. Manea, I.; Razvan Iacob, R.; Iacob, S.; et al. Liquid biopsy for early detection of hepatocellular carcinoma. *Front. Med.* **2023**, *10*, 1218705. [CrossRef]
36. Xu, X.; Li, Y.X.; Wu, Y.L.; et al. Increased ATF2 expression predicts poor prognosis and inhibits sorafenib-induced ferroptosis in gastric cancer. *Redox Biol.* **2023**, *59*, 102564. [CrossRef]
37. Feng, J.; Hu, J.J. Xia, Y.; et al. Identification of RAD54 homolog B as a promising therapeutic target for breast cancer. *Oncol. Lett.* **2019**, *18*, 5350–5362. [CrossRef]
38. Geng, T.T.; Li, M.; Chen, R.; et al. Impact of GTF2H1 and RAD54L2 polymorphisms on the risk of lung cancer in the Chinese Han population. *BMC Cancer* **2022**, *22*, 1181. [CrossRef]
39. Kondo, N.; Takahashi, A. Mori, E.; et al. DNA ligase IV as a new molecular target for temozolomide. *Biochem. Biophys. Res. Commun.* **2009**, 387, 656–660. [CrossRef]
40. Kaur, E.; Agrawal, R.; Arun, R.; et al. Small molecules that disrupt RAD54-BLM interaction hamper tumor proliferation in colon cancer chemoresistance models. *J. Clin. Invest.* **2024**, *134*, e161941. [CrossRef]
41. Zeng, Y.; Luo, C.L.; Lin, G.W.; et al. Whole-exome sequencing association study reveals genetic effects on tumormicroenvironment components in nasopharyngeal carcinoma. *J. Clin. Invest.* **2025**, *135*, 182768. [CrossRef]
42. Nguyen, N.H.K.; Rafiee, R.; Tagmount, A.; et al. Genome-wide CRISPR/Cas9 screen identifies etoposide response modulators associated with clinical outcomes in pediatric AML. *Blood Adv.* **2023**, *7*, 1769–1783. [CrossRef]